D. Tedeschi,[‡,⊥] M. De Luca,[‡,⊥,+] H. A. Fonseka,[^] Q. Gao,[^] F. Mura,[#] H. H. Tan,[^] S. Rubini,[§] F. Martelli,[Δ] C. Jagadish,[^] M. Capizzi,[‡] and A. Polimeni[‡,*]

[‡]Dipartimento di Fisica, Sapienza Università di Roma, Piazzale A. Moro 2, 00185 Roma, Italy

[^]Department of Electronic Materials Engineering, Research School of Physics and Engineering, The Australian National University, Canberra, ACT 2601, Australia

[#]Dipartimento di Chimica and Sapienza Nanoscience & Nanotechnology Lab (SNN-LAB), Sapienza Università di Roma, Piazzale A. Moro 2, 00185 Roma, Italy

[§]Istituto Officina dei Materiali CNR, Basovizza SS 14 km 163.5, 34149 Trieste, Italy

[Δ]Istituto per la Microelettronica e i Microsistemi CNR, Via del fosso del cavaliere 100, 00133 Roma, Italy

ABSTRACT Heat management mechanisms play a pivotal role in driving the design of nanowire (NW)-based devices. In particular, the rate at which charge carriers cool down after an external excitation is crucial for the efficiency of solar cells, lasers, and high-speed transistors. Here, we investigate the thermalization properties of photo-generated carriers by continuous-wave (cw) photoluminescence (PL) in InP and GaAs NWs. A quantitative analysis of the PL spectra recorded up to 310 K shows that carriers can thermalize at a temperature much higher than that of the lattice. We find that the mismatch between carrier and lattice temperature, ΔT, increases exponentially with lattice temperature and depends inversely on the NW diameter. ΔT is instead independent of other

NW characteristics, such as crystal structure (wurtzite *vs* zincblende), chemical composition (InP *vs* GaAs), shape (tapered *vs* columnar NWs), and growth method (vapor-liquid-solid *vs* selective-area growth). Remarkably, *carrier* temperatures as high as 500 K are reached at the *lattice* temperature of 310 K in NWs with ~70 nm diameter.

While a population of non-equilibrium carriers, usually referred to as "hot carriers", is routinely generated by high-power laser pulses and detected by ultrafast spectroscopy, it is quite remarkable that it can be observed in cw PL measurements, when a steady-state population of carriers is established. Time-resolved PL measurements show that even in the thinnest NWs carriers have enough time (~1 ns) after photo-excitation to interact with phonons and thus to release their excess energy. Nevertheless, the inability of carriers to reach a full thermal equilibrium with the lattice points to inhibited phonon emission primarily caused by the large surface-to-volume ratio of small diameter NWs.

KEYWORDS InP and GaAs nanowires, hot carriers, photoluminescence, zincblende, wurtzite.

Introduction. Unlike bulk materials, nanowires (NWs) offer unprecedented opportunities to manipulate the thermal properties of semiconductors at the nanoscale, thus providing access to a variety of size-dependent effects. For instance, growing Si in the NW form has increased the rate of phonon scattering, thus hampering heat flow and boosting the thermoelectric properties of Si.[1] This observation is related to the anisotropic shape and typical dimensions of NWs that permit the exploitation of phonon-scattering elements at different length scales. For instance, the NW surface is an important scattering element for phonons whose wavelength is comparable to the NW diameter.[2] Moreover, shorter-wavelength phonons are efficiently suppressed by introduction of impurities[3] or controlled roughness along the NW surface.[4] Finally, mass fluctuations induced by isotopic disorder may also act as strong phonon-scattering elements.[5]

While the feasibility to tailor phonon scattering rates in NWs has been extensively investigated by different means,[1,2,3,4,5] the influence of this scattering on carrier-phonon interaction is still almost unexplored despite its relevance for the new generation of electronic and optoelectronic devices. In these applications, hot electrons and hot holes are typically generated by light absorption or by injection at the contacts. These charge carriers are named *'hot carriers'* because they gain a large amount of kinetic energy due to the external excitation that provides them with energy higher than that of the band gap. A carrier temperature can be defined soon after external excitation (<100 fs), when very fast carrier-carrier scattering processes bring electrons and holes into an energy distribution with an effective temperature.[6] Typically, this temperature is higher than that of the ions vibrating in the lattice (T_L), namely the crystal temperature. Then, in few ps after excitation, hot carriers relax towards the band edges and dissipate their excess energy by phonon emission, thus reaching a thermal equilibrium with the underlying lattice. Finally, after hundreds of ps electrons and holes recombine. In these processes, carrier-phonon interaction is pivotal as it determines the rate at which hot carriers relax after the excitation.

Hot carriers may be either detrimental or desirable, depending on applications. In interband semiconductor lasers, it is advantageous to promote the carrier-phonon interaction to accelerate carrier relaxation and reduce hot carrier effects. In other cases, such as in mid-infrared lasers based on intraband transitions[7] and photodetectors,[8] a weak electron-phonon interaction is preferred, as it leads to an increase in the lifetime of the excited states involved or allows thermal decoupling of electrons from the phonon bath. In photovoltaic applications, where typically a certain amount of the hot carrier energy is irreversibly lost because of the cooling process,[9] it is often convenient, though challenging, to capture hot carriers before they relax to the band edges. This could be attained, for instance, by creating a *'phonon bottleneck'* able to maintain the hot carrier population for a longtime.[6,10] Such a phonon bottleneck can be built by resorting to quantum structures, whose spacing between the discrete electronic states is larger than the highest phonon frequency, or by producing the so called *'hot phonons'*. This term is broadly used to indicate a high-density of

phonons[11,12] that cannot equilibrate fast enough with the crystal bath and are continuously reabsorbed by the carrier ensemble, which is thus re-heated.

In semiconductor NWs, the presence of hot carriers was investigated in *transistors*,[13,14,15,16] where a plasmon-mediated hot electron injection was also recently explored.[17] The *optical* generation and detection of hot carriers in NWs, however, was studied in only two works[18,19] by ultrafast optical spectroscopy under intense excitation, which is the most commonly used technique to investigate hot carriers that typically lose most of their excess energy over ps timescales.

Here, we unveil the existence of long-lived hot carriers in NWs under the quasi-equilibrium conditions provided by *continuous wave*, *cw*, photoluminescence (PL). The use of PL under steady state allows us to minimize the many-body effects usually associated with hot carriers in bulk semiconductors excited by very intense laser pulses. We have performed measurements from 80 to 310 K on InP and GaAs NWs. Eleven different NW samples have been studied, with diverse NW shapes (tapered *vs* untapered, columnar *vs* kinked, hexagonal *vs* square cross-sections), crystal structures [zincblende (ZB), *vs* wurtzite (WZ)], growth method and technique [vapor-liquid-solid growth (VLS) *vs* metal-free selective-area epitaxy (SAE); molecular beam epitaxy (MBE) vs metal-organic vapor-phase epitaxy (MOVPE)], defect densities, and surface quality. The carrier temperature (T_C) is determined by a quantitative analysis of the emission spectrum line shape. Notably, we observe that the carrier temperature in thin nanowires is much higher than the lattice temperature. In particular, the temperature difference, $\Delta T=T_C-T_L$, increases with decreasing NW diameter, regardless of any other NW characteristic, and, at a fixed NW diameter, it increases exponentially with increasing lattice temperature.

Morphological and Structural Properties of the Samples. We investigated mainly InP nanowires as they represent a model system in which great control of the growth conditions has been reached through different techniques.[20,21,22,23] Moreover, strong PL signals are observed up to room temperature (RT)[20,21,22,24,25] and the relationship between structural and optical properties is well

established, from both the experimental[20,21,22,23,24,26,27,28,29,30] and theoretical[31,32,33] point of view. This makes the quantitative analysis of PL line shapes more robust because the fundamental parameters entering into the fitting procedures can be readily compared with existing results in literature. Moreover, InP NWs are a suitable material system for photovoltaic applications.[34]

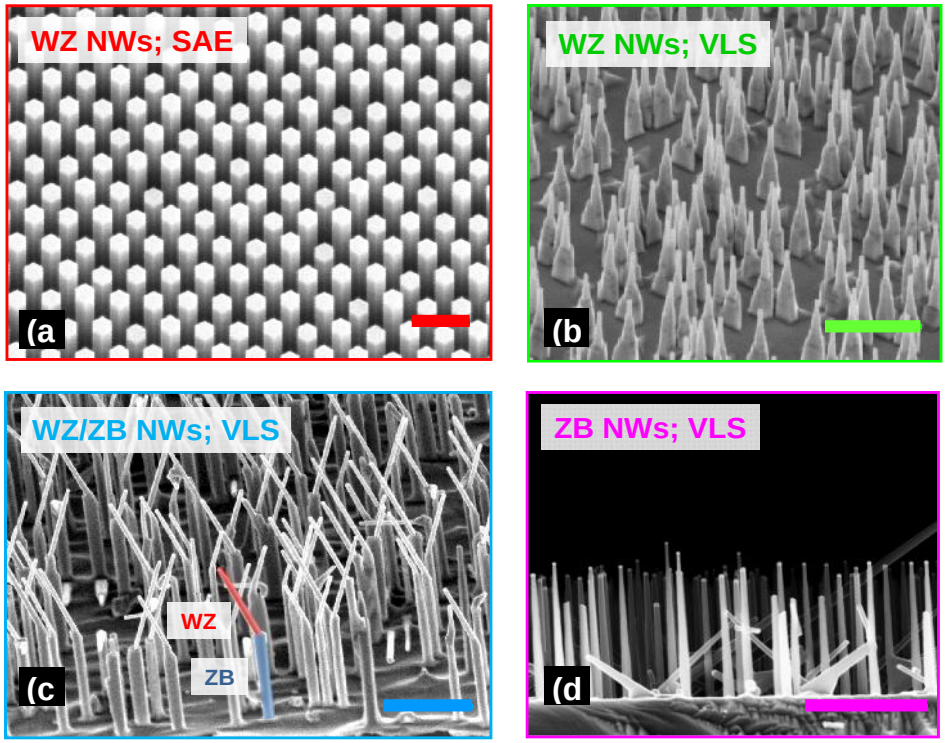

Figure 1 SEM images of some representative InP NW ensembles. Scale bars are 1 µm. (a) Tilted-view image of NWs grown by metal-free SAE and having pure WZ structure. (b) Tilted-view image of tapered WZ NWs grown by Au-seeded MOVPE. (c) Tilted-view image of untapered NWs grown by Au-seeded MOVPE. The vertical segment (blue colored area) has ZB structure, the inclined one (red colored area) has WZ structure. (d) Side-view image of slightly tapered ZB NWs grown by Au-seeded MOVPE. A small percentage of inclined WZ NWs can be observed.

An overview of the morphological characteristics of some representative InP NW ensembles is given by the scanning electron microscope (SEM) images shown in the four panels of Figure 1. All NWs were grown on InP substrates. Panel (a) shows an array of NWs grown by SAE along the <111> direction. The substrate was covered with a thin SiO_2 layer patterned with an array of holes where the NW nucleation took place. We designed four patterns with different hole diameters (45, 120, 310, and 650 nm) to grow NWs with different diameter. For clarity, in panel (a) only the sample with hole diameter of 310 nm is shown. Apart from the hole diameter, all growth parameters

are the same for the four samples and are provided in S1)1.a) in the Supporting Information. The four SAE NW samples feature the same morphological characteristics, namely, the NWs are untapered, ~5 µm-long, perfectly vertical on the substrate, equally spaced and have hexagonal cross-section. They have a defect-free WZ crystal structure, as demonstrated by high-resolution transmission electron microscopy (TEM) and selected-area electron diffraction.[22]

The growth of the NWs shown in panels (b), (c), and (d) was carried out using the standard Au-seeded VLS-MOVPE. Growth details of the three samples are provided in S1)1.b), c), and d). Panel (b) displays an ensemble of NWs with WZ structure showing some stacking faults in the tip regions only.[29,30] These NWs are grown along the <111> direction. They are highly tapered (with approximate tip and base diameters of 30 and 200 nm, respectively), ~1 µm-long, and have a hexagonal-truncated triangular cross-section.[29,30] Panel (c) shows an ensemble of kinked NWs. Each of them is formed by a ~1.4 µm-long vertical segment oriented along the <100> direction (the average size of the side of the square cross-section is ~120 nm) followed, after an inclined twin, by a ~1.4 µm-long <111> oriented segment with a 70 nm-wide average hexagonal section. The <100> oriented segment before the twin is of pure ZB phase and the <111> oriented segment is of pure WZ phase; both are almost untapered.[35] Panel (d) displays an ensemble of NWs featuring a pure ZB structure.[25] Most of the NWs are vertical on the substrate along the <100> direction, ~1 µm-long, and slightly tapered. The sides of the square cross-section are 70 nm-long at the NW base and 45 nm at the tip. There are also few non-vertical wires, most of which are WZ NWs growing in the <111> directions.[35]

In addition, we measured $In_xGa_{1-x}As$/GaAs core/shell NWs with x=0.30. These NWs were grown by Au-seeded MBE according to a VLS mechanism on a GaAs substrate, as described in S1) 2. The $In_xGa_{1-x}As$ core is surrounded by a GaAs shell, and a GaAs tip with almost pure WZ phase elongates for ~800 nm on top of the core/shell structure. The GaAs tip has a hexagonal cross-section with constant width of ~120 nm. SEM and TEM images can be found in References 36 and 37, where further growth details are reported. From now on, these NWs will be referred to as 'WZ

GaAs' NWs because we extracted carrier temperature in the spectrum emitted by the WZ GaAs tips only.[36,37]

In the remainder of this paper and for all NWs, we will report as NW 'diameter' (*d*) an effective cross-section of the NW. This quantity is determined as an average between the diameters of the circumferences inscribed-in and circumscribed-to the NW hexagonal or square section measured by SEM. In case of tapered wires, each section featuring a different *d* value was weighted by the corresponding volume (to a first approximation PL signals are indeed proportional to the volume of the emitting region). In case of single wire measurements, the diameter is the exact diameter of the probed NW. In case of ensemble measurements, *d* has been derived by analyzing the SEM images of tens of NWs. Finally, high-quality InP and GaAs epilayers were investigated for comparison purposes. Growth details are given in S1) 3. The most salient characteristics of the thirteen investigated samples, NWs and epilayers, are summarized in Table S1 in the Supporting Information.

Experimental setup. PL was excited by a cw frequency-doubled Nd:YVO_4 laser (λ=532 nm). In the macro-PL configuration large *ensembles* of NWs were probed, with the laser spot focused to a diameter of ~200 µm. Samples were measured at different temperatures (10-310 K) by using a He closed-cycle cryostat and PL was collected in a backscattering configuration. In the micro-PL (µ-PL) configuration, the laser was focused by a 50× microscope objective having a 0.55 numerical aperture (measured spot diameter 0.8 µm) that enabled the study of single NWs. The luminescence was collected by the same objective in a backscattering configuration. Samples were measured at different temperatures (80-310 K) by using a liquid N_2-flow cryostat. NWs were moved by computer-driven piezoelectric translation stages with minimum step of 50 nm. In both macro- and µ-PL geometries, PL signals were dispersed by a 0.75 m-long monochromator equipped with a 300 grooves/mm grating blazed at 1 µm, and detected by a liquid N_2-cooled Si CCD. In the time-resolved PL configuration, single NWs were excited using a frequency doubled Yb:YAG laser

(λ=522 nm) with a pulse duration of 300 fs, at 20.8 MHz repetition rate. The laser beam was focused through a 60× microscope objective lens with numerical aperture of 0.7. The emission was detected by a single photon avalanche diode, which was connected to a Picoharp 300 time-correlated single photon counting system. In the case of NWs standing vertically on the growth substrate, laser and PL collection directions were parallel to the NW growth axis. In the case of NWs lying on a Si substrate, laser and PL collection directions were perpendicular to the NW growth axis. SEM was performed with a FEI Helios 600 NanoLab FIB system. A JEOL 2100F system operated at 200 kV and a Philips CM 300 system operated at 300 kV were used for TEM analysis.

Experimental results and data analysis. Figure 2 (a) and 2 (b) show μ-PL spectra (thick colored lines) recorded from 90 to 310 K on nanowires lying on Si and dropcasted from arrays of WZ InP NWs grown by SAE similar to those displayed in Figure 1 (a). The diameters of the measured NWs are d=125 nm [panel (a)] and d=700 nm [panel (b)], as determined by the SEM images in panel (c). Apart from the line width, the PL spectra of the two NWs exhibit similar characteristics. The emission peak at 1.482 eV in the spectra recorded at the lattice temperature T_L=90 K is due to the band-gap free-exciton (FE). It corresponds to optical transitions from the minimum of the lowest conduction band (CB), with symmetry Γ_7^C, to the valence band (VB) maximum with symmetry Γ_9^V. We label this transition as A following the terminology used for WZ crystals. The nature of this recombination evolves from excitonic to band-to-band with increasing T_L, due to exciton thermal dissociation.[25] With increasing temperature, the spectrum broadens asymmetrically and the Boltzmann-like tail on the high-energy side becomes more pronounced. For $T_L \geq 130$ K, a band at energy about 40 meV above A appears as a result of thermal population. This band, labeled B, is due to transitions from the CB minimum to the second VB maximum, with symmetry Γ_{7u}^V.[25,30] Remarkably, band B appears to be much more intense in the sample with d=125 nm than in that

with d=700 nm. Furthermore, at T_L=310 K the weight of band B in the d=125 nm NW exceeds that of band A, pointing to a quite high carrier temperature in this sample. For both NWs, carrier temperature T_C was determined by quantitative analysis of the PL spectra resulting in the fits shown in panels (a) and (b) by dashed black lines. The fitting procedure will be detailed in Figure 3 for various samples.

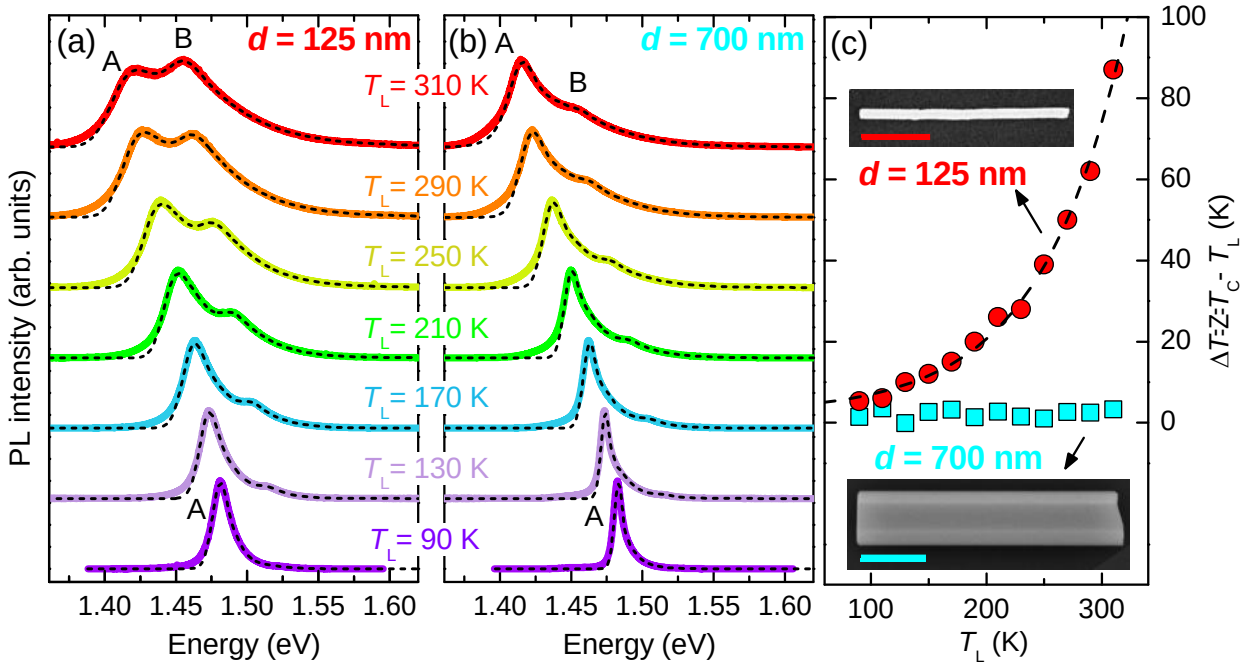

Figure 2 (a), (b) µ-PL spectra (thick colored lines) recorded at the indicated lattice temperature T_L on single InP NWs lying on a Si substrate. NWs were grown by metal-free SAE. Dashed black lines are fits to the spectra; the small mismatch between data and fits on the low-energy side is due to contribution from defect states not considered in the fits. The spectra in (a) were recorded on a representative NW with d=125 nm at power density P =1.14 kW/cm^2; the spectra in (b) were recorded on a representative NW with d=700 nm at P=0.51 kW/cm^2. SEM images of both NWs are in (c) –scale bars are 1 µm. (c) Difference between carrier and lattice temperatures, $\Delta T = T_C - T_L$, as a function of T_L for the NW with d=125 nm (red circles) and the NW with d=700 nm (light blue squares). The dashed line for d=125 nm is an exponential fit.

Figure 2 (c) displays the difference between carrier and lattice temperatures, $\Delta T = T_C - T_L$, as a function of T_L. Dramatically different behaviors are found for NWs with different diameters. ΔT is essentially zero in the d=700 nm sample at every T_L (light blue squares), while it increases exponentially with increasing T_L in the d=125 nm sample (red circles and dashed line), becoming almost 90 K at T_L=310 K. The very similar carrier and lattice temperature found for d=700 nm indicates that charge carriers recombine after having fully transferred to the lattice their excess

kinetic energy *via* phonon emission. On the contrary, such a kinetic energy-to-heat conversion is much less efficient for *d*=125 nm, thus resulting in recombination of carriers whose temperature is higher than that of the lattice. This finding is notable: hot carriers are observed here under cw laser excitation, namely, in steady-state *quasi-equilibrium* conditions, provided the NW diameter is small enough. All other characteristics of the two NWs are, in fact, very similar: growth method and parameters, morphological properties, and crystal (surface and bulk) quality. Further evidence of this carrier temperature dependence on NW diameter will be provided in the following for all investigated samples.

An important clarification concerning lattice temperature is now in order. It is well known that laser beams focused through microscope objectives may lead to high power densities and act as local heat sources, with an ensuing increase in lattice temperature. Therefore, a tight control of T_L during our experiments is essential to exclude an increase in T_C due to a trivial lattice heating. The well-established dependence on lattice temperature of the band-gap energies (E_g) in WZ and ZB InP[25] allows us to determine T_L independently and univocally from a line shape analysis of each PL spectrum, as illustrated below. The uncertainty in the estimation of E_g varies from 0.1 meV (at 90 K) to 1 meV (at 310 K). This leads to an uncertainty on T_L ranging from 0.5 K (at 90 K) to 3.0 K (at 310 K) that is smaller than the symbol size in Figure 2 (c). In our measurements, the estimated T_L values agree perfectly with those that were set on the sample stage, thus proving that laser heating is negligible for all the used power densities (<30 kW/cm^2). Therefore, all T_L values provided henceforth correspond to the actual temperatures of the lattice.

As for carrier temperature, this quantity was accurately determined at a fixed lattice temperature by performing a fit of the *whole* PL line shape. The PL spectrum is given by[38]

$$I_{PL} \propto \sim(\hbar\mu)\, f_e(\hbar\mu)\, f_h(\hbar\mu), \quad (1)$$

where $\sim(\hbar\mu)$ is the absorption coefficient, whose expression is provided in S2) in the Supporting Information. It includes both exciton and band-to-band contributions.[25,39] $f_e(\hbar\mu)$ and $f_h(\hbar\mu)$ are

the Fermi-Dirac distributions for electrons and holes accounting for the thermal population of states. Each function is expressed in terms of carrier quasi-Fermi energy and temperature. The Fermi-Dirac distribution, in steady-state PL measurements, can be set equal for both carriers since electrons and holes usually achieve a common temperature T_C in few picoseconds after excitation.[40] Furthermore, for nondegenerate semiconductors, the Fermi-Dirac function can be approximated by a Boltzmann function, and Eq. (1) becomes[25]

$$I_{PL} \propto \sim (\hbar\mu) e^{-\frac{\hbar\mu}{k_B T_C}} \tag{2}$$

Notice that the slope of the high-energy tail of $\ln[I_{PL}(\hbar\mu)]$ *vs* $\hbar\mu$ does not provide the carrier temperature, as exemplified in Figure S2 b in the Supporting Information. Therefore, we have developed an analysis procedure to fit the *whole* PL line shape *via* Eq. 2.

Figure 3 shows the emission spectra (thick cyan lines) of some representative samples recorded at T_L=310 K and fitted by Eq. 2 (black dashed lines). The carrier temperature and its mismatch with the lattice temperature are also reported in the figure. μ-PL spectra in (a), (b), and (c) were taken on single InP NWs transferred by dropcast onto a Si substrate. Specifically, the spectrum in (a) was recorded on the WZ section (*d*=74 nm) of a kinked NW, whose SEM image is given in Figure 1 (c). We notice that the high carrier temperature observed in this NW allows even the third VB (with symmetry Γ_{7l}^{V}, labeled C) to remain populated.[25,30] The spectrum in (b) was recorded on the ZB section (*d*=139 nm) of another NW from the same sample. Panel (c) concerns a WZ NW with *d*=335 nm belonging to the NW array whose SEM image is shown in Figure 1 (a). A macro-PL spectrum taken on an InP epilayer is displayed in panel (d). In all panels, excitonic ($E_{1,2}$ are the *n*=1,2 exciton states) and band-to-band ($E_{b\text{-}b}$) contributions to the fits are highlighted by blue and orange filled areas, respectively. The same fitting procedure was applied to analyze the PL spectra in Figure 2 (a) and (b), as detailed in Figure S2) in the Supporting Information. There is a very good agreement between experimental data and fits for all samples, with a small disagreement on the low-energy side of the spectra due to defect states not included in the fitting procedure.

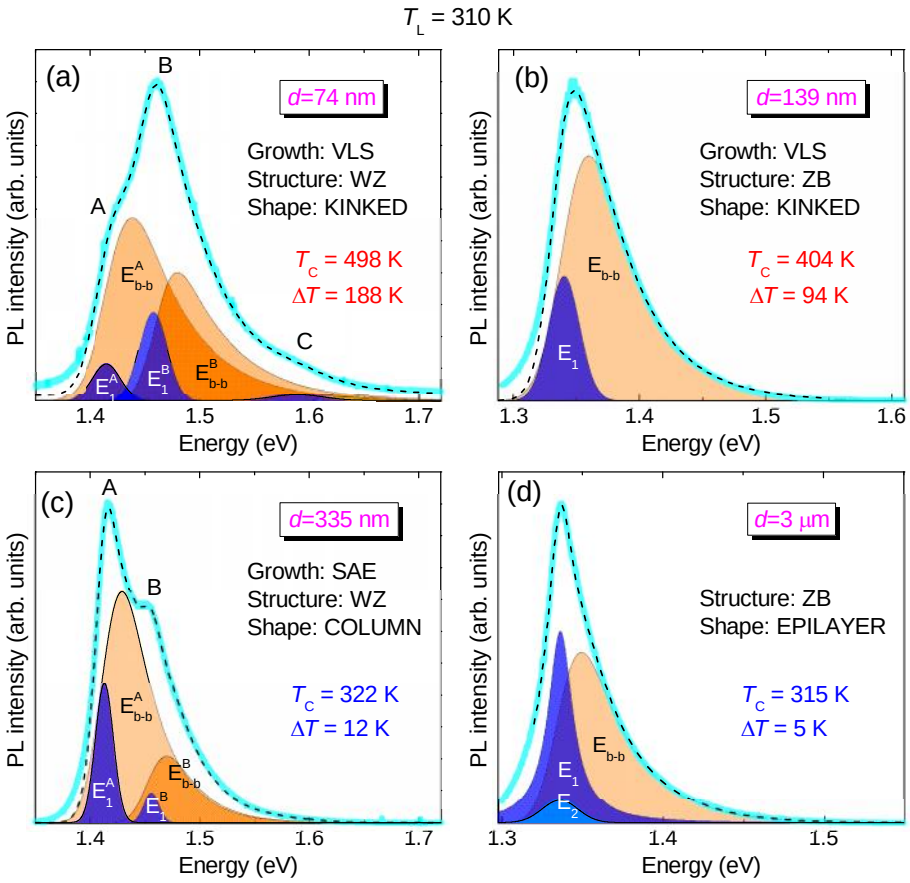

Figure 3 PL spectra (thick cyan lines) recorded at 310 K on single InP NWs lying on Si substrates [panels (a), (b), and (c)] with a μ-PL setup and on an InP epilayer [panel (d)] with a macro-PL setup. Dashed black lines are best fits to the data *via* Eq. 2. The various contributions are indicated by blue-filled areas for exciton transitions (labeled as E_n, with n=1 for the ground state and n=2 for the first excited state) and orange-filled areas for band-to-band transitions (labeled as $E_{b\text{-}b}$). For WZ samples the superscripts A, B, and C associate those contributions to the different transitions involved. Power densities were P =12.7 kW/cm^2 in (a), P =20.4 kW/cm^2 in (b), P =0.7 kW/cm^2 in (c), and P =0.7 W/cm^2 in (d). T_C and ΔT values resulting from the fits are given in each panel.

Results in Figures 3 confirm and enrich the picture emerged from Figure 2: the presence of hot carriers depends on the NW diameter and not on other NW characteristics, such as the growth method or crystal phase. Moreover, the small ΔT values (<15 K at T_L=310 K) given in Figure 2 (c) for d=700 nm and in Figure 3 (c) for d=335 nm, both relative to WZ NWs grown by SAE and having a columnar shape, point to the existence of a diameter (~330 nm) above which the presence of hot carriers disappears.

In order to investigate such a dependence on the NW size in greater detail, PL spectra on all the InP and GaAs samples described in the Experimental section were recorded and compared at a

fixed lattice temperature (T_L=290 K). The reader is referred to Figure S3 in the Supporting Information, where all measurements are shown along with a quantitative analysis of the PL spectra. Figure 4 gives the resulting $\Delta T=T_C-T_L$ as a function of the diameter d (for epilayers, their thickness was used). The main characteristics of the investigated samples are given in the inset and match those reported in Table S1 in the Supporting Information.

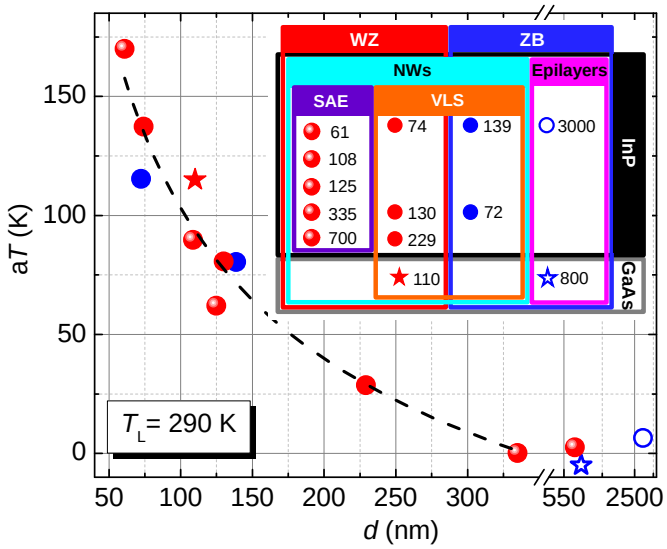

Figure 4 $\Delta T=T_C-T_L$ as a function of the diameter for all InP and GaAs samples listed in Table S1 in the Supporting Information. ΔT was determined by a quantitative analysis of the PL spectra (recorded at T_L=290 K and shown in Figure S3) using Eq. 2, following the procedure described in Figure 3. Notice the x axis break from 350 to 550 nm and the semilog scale after the break. Error bars for ΔT and d are smaller than the symbol size. The dashed line is a hyperbolic fit to the d<350 nm data. The characteristics of the investigated samples are summarized in the inset, where numbers are diameters in nm.

The two epilayers were measured with the macro-PL setup. PL measurements on all SAE samples and on the VLS NWs with d=74 and 139 nm were performed with the μ-PL setup on single wires. VLS-grown NWs with d=72, 130, 229, and 110 nm were instead measured in the ensemble configuration with the macro-PL setup. Within this group of NWs, we point out that d=130 nm and d=110 nm NWs are NWs vertically standing on their growth substrate, while d=72 and d=229 NWs are mechanically transferred on a Si substrate. SAE NWs with d=335 and d=700 nm were measured also in the ensemble configuration, and a ΔT value equal to the one found in the single wire measurements was obtained. Figure 4 validates and strengthens the results in Figure 3. ΔT depends *only* on the NW diameter and increases as 1/d. This increase is independent of the experimental

configuration and of any other NW characteristic, such as crystal composition, NW shape, crystal structure, and growth method. ΔT approaches zero above d ~330 nm.

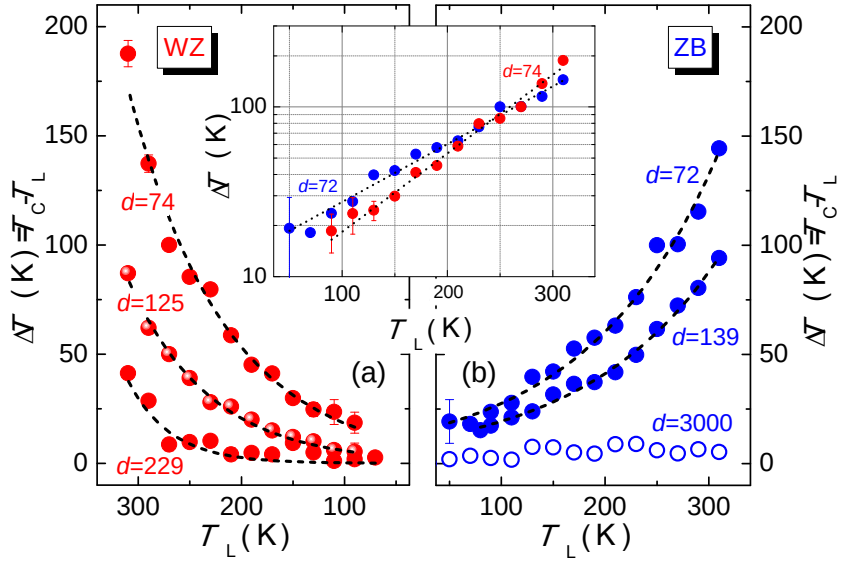

Figure 5 $\Delta T=T_C-T_L$ *vs* T_L for InP NWs with WZ and ZB structure in (a) and (b), respectively. Black dashed lines are exponential fits to the data. The inset shows ΔT *vs* T_L on a semilog scale for a sample with WZ structure (d=74 nm, red circles) and a sample with ZB structure (d=72 nm, blue circles).

Furthermore, we examined the dependence of the thermal budget of carriers on lattice temperature to gain further insight into the presence of hot carriers in NWs. We recorded PL spectra in the T_L=80-310 K range on several samples and, at each T_L, we determined the T_C values. Figure 5 shows the resulting ΔT as a function of T_L for representative InP samples with WZ [panel (a)] and ZB [panel (b)] crystal structures. The diameter labeling each curve (as well as the used symbols) allows tracing the sample properties by using Table S1 in the Supporting Information and the inset in Figure 4. At a fixed T_L, ΔT increases with decreasing NW diameter. Moreover, as anticipated in Figure 2 (c), ΔT increases *exponentially* with increasing T_L in *all* WZ and ZB NW samples exhibiting hot carriers. Carrier temperatures as high as 500 K are reached at T_L=310 K for d=74 nm. The experimental data are empirically reproduced by $\Delta T(T_L) = C\,e^{DT_L}$ (dashed lines in Figure 5) with C and D free parameters. Within the group of NWs with the same crystal structure, a smaller diameter leads to a greater increase in ΔT, namely to larger C. In WZ structures, for instance, C varies from 0.3 ± 0.2 K to 7.1 ± 5.9 K when d decreases from 229 to 74 nm. On the other hand, the

values of D are similar in NWs with the same crystal structure, with a slightly larger value in WZ compared to ZB. For instance, the inset in Figure 5 displays ΔT *vs* T_L for a WZ (red circles) and a ZB (blue circles) sample with similar diameters (~70 nm) on a semilog scale. The line associated with the WZ sample exhibits a slightly greater slope, namely, $D=(10.0\pm 2.61)\times10^3$ K^{-1} in WZ and $(7.5 \pm 1.5)\times10^3$ K^{-1} in ZB. The small differences in the rate of increase in ΔT between WZ and ZB NWs might be due to the different WZ and ZB phonon dispersion curves.[41]

Discussion. We now address possible explanations of the results reported so far. As mentioned in the introduction, the presence of hot carriers in NWs has been optically detected so far only in highly excited semiconductors.

In Ref. 18, hot carrier dynamics in ensembles of polytypic InP NWs, namely wires with WZ crystal structure containing ZB inclusions, was investigated by room temperature PL generated by fs laser pulses and resolved on a ps timescale. As commonly observed in highly excited semiconductors, T_C decreases in a few ps after the excitation pulse. During that transient, a sizable increase in carrier temperature with respect to the lattice temperature was observed in NWs with small diameter (50 nm). This hot carrier effect persisted for several tens of ps after the laser pulse and was attributed to inefficient carrier cooling caused by crystal phase disorder.[18] Interestingly, the ΔT values extrapolated from Figure 4 (b) in Ref. 18 for thin NWs are consistent with those estimated in the present work, where, however, politypism is absent. This suggests that a significant role could be played by the diameter also in the results presented in Ref. 18.

Single InP and GaAs NWs were studied in Ref. 19 by low-temperature transient Rayleigh scattering, once again under high excitation. Therein, hot phonons were invoked to account for an electron-hole plasma temperature higher than that of the lattice. Such an out-of-equilibrium phonon population cannot explain our results. Indeed, typically hot phonon presence is negligible in steady-

state measurements due to the small number of photo-generated carriers and the ensuing small number of phonons emitted during carrier relaxation.

We have monitored the possible presence of hot phonon effects by studying the dependence of carrier temperature on excitation power density, which is proportional to the photo-generated carrier density. As shown in Figure S4 in the Supporting Information, at a given lattice temperature the PL line shape (and thus band gap energy and carrier temperature) does not vary with power density. This applies independently of the presence of hot carriers (namely, of NW diameter). As already discussed, unchanged band gap energy at all powers indicates constant T_L and allows excluding any lattice heating induced by laser. Incidentally, we can also rule out non-trivial size effects that may influence the extent of light absorption in the NWs and hence the amount of power collected by them thus leading to lattice heating.[42,43] Indeed, in the experiments reported in S4 in the Supporting Information, the laser power density was varied up to a factor 100 (14) for vertically standing (horizontally lying) NWs without any sizable increase in carrier temperature. These factors are well within the expected absorption enhancements calculated in Refs 42 and 43.

Most importantly, the absence of any increase in T_C values with increasing photo-generated carrier density excludes possible non-equilibrium phonon population. Auger effect[44] can also be excluded, since its observation is more likely under extremely high carrier densities in small nanostructures, where spatial confinement leads to a strong overlap between electron and hole wave-functions. These conditions are not satisfied in our NWs that have rather large diameters (d>50 nm) and are excited at low power density.

We also performed time-resolved PL measurements to examine one more possible effect. It is known that recombination from hot carriers can be observed when carrier lifetime is shorter than (or comparable to) the relaxation time necessary for an energy transfer to the lattice (1-100 ps).[40] Moreover, it has been demonstrated that carrier recombination time in NWs ($^2_{NW}$) depends on NW diameter according to the relation[45]

$$\frac{1}{\tau_{NW}} = \frac{1}{\tau_{bulk}} + \frac{4S}{d}, \tag{3}$$

where τ_{bulk} is the carrier lifetime in the bulk material and S is the surface-recombination velocity. Therefore, smaller diameters should correspond to shorter τ_{NW} and, whenever these τ_{NW}'s are so small to fall in the timescale of the phonon-assisted thermalization processes, hot carriers should be observed because electrons and holes do not have sufficient time to release their excess energy to the lattice.

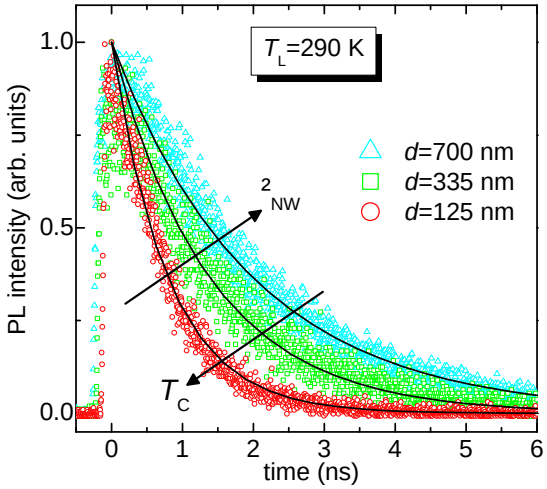

Figure 6 Transient μ-PL decays (colored symbols) of single SAE-grown WZ InP NWs with the indicated diameters. PL signals were recorded at lattice temperature of 290 K and power density of 16 W/cm^2, and detected at the band gap energy. Carrier lifetimes as determined by single-exponential decay fits (thick black lines) are τ_{NW}=0.82±0.01 ns for d=125 nm, τ_{NW}=1.39±0.01 ns for d=335 nm, and τ_{NW}=1.98±0.01 ns for d=700 nm.

We then resorted to time-resolved PL spectroscopy to investigate the diameter-dependence of τ_{NW} (if any) and, most importantly, to find out whether carrier recombination time was close to the ps timescale. This experiment was performed at T_L=290 K on NWs with diameters d=125, 335, and 700 nm (namely, larger and smaller that the 330 nm threshold above which hot carriers are absent) singled out from different ensembles of the WZ NWs grown by SAE. The spectra were recorded at the PL peak energy and up to few tens of ns after the laser pulse. Figure 6 shows the transient μ-PL decay data (colored symbols), as well as single-exponential decay fits (thick black lines). Carrier lifetimes are τ_{NW}=0.82±0.01 ns for d=125 nm, τ_{NW}=1.39±0.01 ns for d=335 nm, and

$^{2}_{NW}$=1.98±0.01 ns for *d*=700 nm. As expected, $^{2}_{NW}$ decreases monotonically with decreasing *d*. However, even in the *d*=125 nm sample, $^{2}_{NW}$ is too long to be comparable with carrier relaxation times and thus to account for the hampered heat dissipation we have reported on.

These studies demonstrate that several common explanations for the hot carrier occurrence do not apply to our results. In our samples, hot phonons are negligible and carriers do have enough time to dissipate the excess energy provided by the laser excitation. In this picture, the reduced heat dissipation we have observed in small NWs could be ascribed either to a reduced carrier-phonon interaction or to an inhibited phonon emission, which calls for further theoretical investigation.

Here, we notice that thermal conductivity, ©, measurements in several NW systems, such as ZnO NWs[46] and InAs NWs[47], evidenced that © decreases with decreasing NW diameter, thus prompting an experimental phenomenology that resembles the diameter dependence of T_C displayed in Figure 4. In NWs, the reduced thermal conductivity as compared to bulk is usually ascribed to a suppression of available phonon modes due to the modified phonon density of states in 1D and phonon scattering by various elements.[1,2,4,48] On the ground of this experimental similarity, we suggest that the mechanisms that impede heat flow (*i.e.*, dissipation) in NWs play a major role also in preventing photogenerated carriers from releasing their excess energy by phonons. In our NWs whose diameter ranges from 60 to 700 nm, phonon confinement (and resulting modification of the density of states) is negligible.[48] In general, the most important phonon scattering elements are provided by temperature-dependent phonon-phonon and umklapp processes, and by temperature-independent interaction with impurities, line defects, roughness, and boundaries.[46,49] Among the *T*-independent processes, we can neglect contributions from point and interface defects because we have observed hot carriers in samples grown by different methods and having different crystal quality. Also, we can disregard major contributions from rough surfaces, because high-resolution TEM images taken close to the surface of several NW samples (see Figure S5 in the Supporting Information) do not display very rough surfaces and, most importantly, there is no correlation

between roughness and diameter. Therefore, the observation of a dependence of hot carriers on NW diameter points to the NW surface itself as the most effective phonon-scattering element, as if the phonons that are mainly involved in the relaxation of photo-generated carriers in InP and GaAs NWs were those whose mean free path is comparable to the NW diameter. As a matter of fact, the rate of boundary scattering of phonons depends on the inverse of the NW diameter.[49] Within this picture, the smaller the diameter and the hotter the carriers are (because of a scattering-induced suppression of the phonons that are diffused by boundaries).

Finally, the increase of ΔT with T_L shown in Figure 5 is consistent with the increased umklapp and phonon-phonon scattering rates with lattice temperature highlighted by thermal conductivity experiments on NWs.[46,49] Likewise the mechanism envisaged for the dependence of T_C on the inverse of d, we can only qualitatively liken the drastic reduction of thermal conductivity for T_L>150 K[46,49] to the carrier temperature increase with lattice temperature in our NWs. Although a purely exponential law with temperature (such as that we find) was neither found[46] or predicted[49] for phonon-phonon and umklapp scattering rates, the experimental results here reported should stimulate thorough theoretical studies of the complicated temperature-dependent interplay between diffuse boundary scattering, phonon-phonon scattering, and carrier-phonon interaction.

Conclusions. We have employed cw PL spectroscopy to investigate the thermalization properties of photo-generated carriers in InP and GaAs NWs with different structural and morphological characteristics. By a quantitative analysis of the PL spectra, we find evidence of hot carriers, whose temperature can exceed largely that of the lattice. In particular, the difference between carrier and lattice temperature increases dramatically (from 0 up to 190 K) with increasing lattice temperature (from 80 to 310 K) and decreasing NW diameter (from 700 to 60 nm), independently of all the other NW characteristics (crystal structure, chemical composition, shape, and growth method). Usually, hot carriers are found within few ps after excitation. Instead, here we observe this phenomenon in the steady-state regime, most likely because the large surface-to-volume ratio of

small diameter NWs prevents carriers from reaching the thermal equilibrium with the lattice via phonon emission. On the other hand, time-resolved PL measurements show that hot carriers live long enough (1 ns) to ensure that interaction dynamics with phonon modes can take place, and thus confirm that the presence of hot carriers is an intrinsic feature of thin NWs. The ability of charge carriers to harvest a thermal budget for the long-time probed by steady-state PL spectroscopy (and at the temperatures useful for practical devices) could be of great relevance for photovoltaic and thermoelectric applications.

ASSOCIATED CONTENT

Supporting Information. Supporting material provides growth and structural details of all samples and shows photoluminescence measurements at different power densities and lattice temperatures. Details on the quantitative analysis of the emission spectra are also provided.

AUTHOR INFORMATION

Corresponding Authors

*E-mail addresses: antonio.polimeni@roma1.infn.it

[+]Present address: Department of Physics, University of Basel, Klingelbergstrasse 82, 4056 Basel, Switzerland

Author Contributions

[⊥]These authors contributed equally to this work.

Notes

The authors declare no competing financial interest.

ACKNOWLEDGEMENTS MDL, DT, and AP acknowledge funding by Sapienza Università di Roma under the “Avvio alla Ricerca 2014”, “Avvio alla Ricerca 2015” and “Ateneo 2013” grants, respectively. AP also acknowledges “Awards 2014” by Sapienza Università di Roma. The authors acknowledge F. Mauri and I. Zardo for fruitful discussions. The authors from the Australian National University acknowledge the Australian Research Council for financial support and Australian National Fabrication Facility and Australian Microscopy and Microanalysis Research Facility for providing access to some of the equipment used in this work.

REFERENCES

[1] Hochbaum, A. I.; Yang, P. *Chem. Rev.* **2010**, *110*, 527-546.

[2] Li, D.; Wu, Y.; Kim, P.; Shi, L.; Yang, P.; Majumdar, A. *Appl. Phys. Lett.* **2003**, *83*, 2934-2936.

[3] Lee, E. K.; Yin L.: Lee, Y.; Lee, W. L.; Lee, S.J.; Cha, S. N.; Whang, D.; Hwang, G. S.; Hippalgaonkar, K.; Majumdar, A.; Yu, C.; Choi, B. L.; Kim, J. M.; Kim, K. *Nano Lett.* **2012**, *12*, 2918-2923.

[4] Hochbaum, A. I; Chen, R.; Delgado, R. D.; Lian, W.; Garnett, E. C.; Najarian, M.; Majumdar, A.; Yang, P. *Nature* **2008**, *451*, 163-167.

[5] Mukherjee, S.; Givan, U.; Senz, S.; Bergeron, A.; Francoeur, S.; de la Mata, M.; Arbiol, J.; Sekiguchi, T.; Itoh, K. M.; Isheim, D.; Seidman, D. N.; Moutanabbir, O. *Nano Lett.* **2015**, *15*, 3885-3893.

[6] Nozik, A. J. *Annu. Rev. Phys. Chem.* **2001**, *52*, 193-231.

[7] Khodr, M. *Res. J. App. Sci. Eng. Technol.* **2015**, *10*, 1384-1388.

[8] Yan, J.; Kim, M-H.; Elle, J.A.; Sushkov, A.B.; Jenkins, G.S.; Milchberg, H.M.; Fuhrer, M.S.; Drew, H.D., *Nat. Nanotech.* **2012**, *7*, 472-478.

[9] Ross, R. T.; Nozik, A. J. *J. Appl. Phys.* **1982**, *53*, 3813.

[10] Conibeer, G.; Shrestha, S.; Huang, S.; Patterson, R.; Xia, H.; Feng, Y.; Zhang, P.; Gupta, N.; Tayebjee, M.; Smyth, S.; Liao, Y.; Lin, S.; Wang, P.; Dai, X.; Chung, S. *Solar Energy Materials & Solar Cells* **2015**, *135*, 124-129.

[11] Van Driel, H. M., *Phys. Rev. B* **1979**, *19*, 5928-5932.

[12] Ridley, B. K., Quantum Processes in Semiconductors, Chapt. 14, *Oxford University Press*, **2013**.

[13] Roddaro, S.; Pescaglini, A.; Ercolani, D.; Sorba, L.; Giazotto, F.; Beltram, F. *Nano Research* **2011**, *4*, 259-265.

[14] Chen, G.; Gallo, E. M.; Leaffer, O. D.; McGuckin, T.; Prete, P.; Lovergine, N.; Spanier J. E. *Phys. Rev. Lett.* **2011**, *107*, 156802.

[15] Yoon, K.; Hyun, J. K.; Connell, J. G.; Amit, I.; Rosenwaks, Y.; Lauhon, L. J. *Nano Lett.* **2013**, *13*, 6183-6188.

[16] Yang, Y.; Peng, X.; Kim, H-S.; Kim, T.; Jeon, S.; Kang, H. K.; Choi, W.; Song, J.; Doh, Y-J.; Yu, D. *Nano Lett.* **2015**, *15*, 5875-5882.

[17] Pescaglini, A.; Martín, A.; Cammi, D.; Juska, G.; Ronning, C.; Pelucchi, E.; Iacopino, D. *Nano Lett.* **2014**, *14*, 6202-6209.

[18] Yong, C. K.; Wong-Leung, J.; Joyce, H. J.; Lloyd-Hughes, J.; Gao, Q.; Tan, H. H.; Jagadish, C.; Johnston, M. B.; Herz, L. M. *Nano Lett.* **2013**, *13*, 4280-4287.

[19] Wang, Y.; Jackson, H. E.; Smith, L. M.; Burgess, T.; Paiman, S.; Gao, Q.; Tan, H. H.; Jagadish, C. *Nano Lett.* **2014**, *14*, 7153-7160.

[20] Vu, T. T. T.; Zehender, T.; Verheijen, M. A.; Plissard, S. R.; Immink, G. W. G.; Haverkort, J. E. M.; Bakkers, E. P. A. M. *Nanotechnology* **2013**, *24*, 115705 1-6.

[21] Alouane, M. H. H.; Chauvin, N.; Khmissi, H.; Naji, K.; Ilahi, B.; Maaref, H.; Patriarche, G.; Gendry, M.; C Bru-Chevallier, C. *Nanotech.* **2013**, *24*, 035704.

[22] Gao, Q.; Saxena, D.; Wang, F.; Fu, L.; Mokkapati, S.; Guo, Y.; Li, L.; Wong-Leung, J.; Caroff, P.; Tan, H. H.; Jagadish, C. *Nano Lett*. **2014**, *14*, 5206-5211.

[23] Li, K.; Sun, H.; Ren, F.; Ng, K. W.; Tran, T.-T.D.; Chen, R.; Chang-Hasnain, C. J. *Nano Lett.* **2014**, *14*, 183-190.

[24] Mishra, A.; Titova, L. V.; Hoang, T. B.; Jackson, H. E.; Smith, L. M.; Yarrison-Rice, J. M.; Kim; Y.; Joyce, H. J.; Gao, Q.; Tan, H. H.; Jagadish, C. *Appl. Phys. Lett.* **2007**, *91*, 263104.

[25] Zilli, A.; De Luca, M.; Tedeschi, D.; Fonseka, H. A.; Miriametro, A.; Tan, H. H.; Jagadish, C.; Capizzi, M; Polimeni, A. *ACS Nano* **2015**, *9*, 4277-4287.

[26] Bao, J.; Bell, D. C.; Capasso, F.; Wagner, J. B.; Mårthensson, T.; Trägårdh, J.; Samuelson, L. *Nano Lett.* **2008**, *8*, 836-841.

[27] Gadret, E. G.; Dias, G. O.; Dacal, L. C. O.; de Lima, M. M. Jr.; Ruffo, C. V. R. S.; Iikawa, F.; Brasil, M. J. S. P.; Chiaramonte, T.; Cotta, M. A.; Tizei, L. H. G.; Ugarte, D.; Cantarero, A. *Phys. Rev. B* **2010**, *82*, 125327.

[28] Perera, S.; Shi, T.; Fickenscher, M. A.; Jackson, H. E.; Smith, L. M.; Yarrison-Rice, J. M.; Paiman, S.; Gao, Q.; Tan, H. H.; Jagadish, C. *Nano Lett*. **2013**, *13*, 5367–5372.

[29] De Luca, M.; Polimeni, A.; Fonseka, H. A.,; Meaney, A. J.; Christianen, P. C. M.; Maan, J. C.; Paiman, S.; Tan, H. H.; Jagadish, C.; Capizzi, M. *Nano Lett.* **2014**, *14*, 4250-4256.

[30] De Luca, M.; Zilli, A.; Fonseka, H. A.; Mokkapati, S.; Miriametro, A.; Tan, H. H.; Smith, L. M.; Jagadish, C.; Capizzi, M; Polimeni, A. *Nano Lett.* **2015**, *15*, 998-1005.

[31] De, A.; Pryor, C. E. *Phys. Rev. B* **2010**, *81*, 155210.

[32] Dacal, L. C. O.; Cantarero, A. *Solid State Commun.* 2011, *151*, 781-784.

[33] Bechstedt, F. and Belabbes, A. *J. Phys.: Condensed Matter* **2013**, *25*, 273201.

[34] Ko, W. S.; Tran, T-T. D.; Bhattacharya, I.; Ng, K. W.; Sun, H.; Chang-Hasnain, C., *Nano Lett.* **2015**, *15*, 4961-4967.

[35] Fonseka, H. A.; Caroff, P.; Wong-Leung, J.; Ameruddin, A. S.; Tan, H. H.; Jagadish, C. *ACS Nano* **2014**, *8*, 6945-6954.

[36] De Luca, M.; Lavenuta, G.; Polimeni, A.; Rubini, S.; Grillo, V.; Mura, F.; Miriametro, A.; Capizzi, M.; Martelli, F. *Phys. Rev. B* **2013**, *87*, 235304 1-8.

[37] De Luca, M.; Polimeni, A.; Felici, F.; Miriametro, A.; Capizzi, M.; Mura, F.; Rubini, S.; Martelli, F. *Appl. Phys. Lett.* **2013**, *102*, 173102 1-5.

[38] Yu, P. Y.; Cardona M., *Fundamentals of Semiconductors*; Springer: Berlin, 2005; pp. 346-354.

[39] Grilli, E.; Guzzi, M.; Zamboni, R.; Pavesi, L. *Phys. Rev. B* **1992**, *45*, 1638-1644.

[40] Shah, J. *Ultrafast spectroscopy of semiconductors and semiconductor nanostructures* **1999,** 115, Springer Science & Business Media.

[41] Gadret, E. G.; de Lima Jr., M. M.; Madureira, J. R.; Chiaramonte, T.; Cotta, M. A.; Iikawa, F.; Cantarero, A. *Appl. Phys. Lett.* **2013**, *102*, 122101.

[42] Cao, L.; White, J. S.; Park, J.; Schuller, J. A.; Clemens, B. M.; Brongersma, M. L. *Nature Mat.* **2009**, *8*, 643-647.

[43] Heiss, M.; Russo-Averchi, E.; Dalmau-Mallorquí, A.; Tütüncüoğlu, G.; Matteini, F.; Rüffer, D.; Conesa-Boj, S.; Demichel, O.; Alarcon-Lladó, O.; Fontcuberta i Morral, A. *Nanotechnology* **2014**, *25*, 014015.

[44] Acherman, M.; Bartko, A. P.; Hollingsworth J. A.; Klimov V. I. *Nature Physics* **2006**, *2*, 557-561.

[45] Leonard, F.; Talin, A. A.; Swartzentruber, B. S.; Picraux, S. T. *Phys. Rev. Lett.* **2009**, 102, 106805 1-4.

[46] Bui, C. T.; Xie, R.; Zheng, M.; Zhang, Q.; Sow, C.H.; Li, B.; Thong, J. T. L. *Small* **2012**, 8, 738-745.

[47] Swinkels, M. Y.; van Delft M. R.; Oliveira, D. S.; Cavalli, A.; Zardo, I.; van der Heijden, R. W.; Bakkers, E. P. A. M. *Nanotechnology* **2015**, *26*, 385401 1-6.

[48] Lü, X.; Chu, J. H.; Shen, W. Z., *J. Appl. Phys.* **2003**, *93*, 1219-1229.

[49] Martin, P.; Aksamija, Z.; Pop, E.; Ravaioli, U. *Phys. Rev. Lett.* **2009**, 102, 125503 1-4.